# Artificial cell membranes interfaced with optical tweezers

## A versatile microfluidics platform for nanomanipulation and mechanical characterization

Dols-Perez, Aurora; Marin, Victor; Amador, Guillermo J.; Kieffer, Roland; Tam, Daniel; Aubin-Tam, Marie Eve

**DOI**
10.1021/acsami.9b09983

**Publication date**
2019

**Document Version**
Final published version

**Published in**
ACS applied materials & interfaces

ACS APPLIED MATERIALS & INTERFACES

Research Article

Cite This: ACS Appl. Mater. Interfaces 2019, 11, 33620−33627

www.acsami.org

# Artificial Cell Membranes Interfaced with Optical Tweezers: A Versatile Microfluidics Platform for Nanomanipulation and Mechanical Characterization

Aurora Dols-Perez,[†,§] Victor Marin,[†,§] Guillermo J. Amador,[†,‡,§] Roland Kieffer,[†] Daniel Tam,[‡] and Marie-Eve Aubin-Tam*[,†]

[†]Department of Bionanoscience, Kavli Institute of Nanoscience, Delft University of Technology, Van der Maasweg 9, Delft 2629 HZ, The Netherlands

[‡]Laboratory for Aero and Hydrodynamics, Delft University of Technology, Delft 2628 CD, The Netherlands

Supporting Information

**ABSTRACT:** Cell lipid membranes are the site of vital biological processes, such as motility, trafficking, and sensing, many of which involve mechanical forces. Elucidating the interplay between such bioprocesses and mechanical forces requires the use of tools that apply and measure piconewton-level forces, e.g., optical tweezers. Here, we introduce the combination of optical tweezers with free-standing lipid bilayers, which are fully accessible on both sides of the membrane. In the vicinity of the lipid bilayer, optical trapping would normally be impossible due to optical distortions caused by pockets of the solvent trapped within the membrane. We solve this by drastically reducing the size of these pockets via tuning of the solvent and flow cell material. In the resulting flow cells, lipid nanotubes are straightforwardly pushed or pulled and reach lengths above half a millimeter. Moreover, the controlled pushing of a lipid nanotube with an optically trapped bead provides an accurate and direct measurement of important mechanical properties. In particular, we measure the membrane tension of a free-standing membrane composed of a mixture of dioleoylphosphatidylcholine (DOPC) and dipalmitoylphosphatidylcholine (DPPC) to be $4.6 \times 10^{-6}$ N/m. We demonstrate the potential of the platform for biophysical studies by inserting the cell-penetrating trans-activator of transcription (TAT) peptide in the lipid membrane. The interactions between the TAT peptide and the membrane are found to decrease the value of the membrane tension to $2.1 \times 10^{-6}$ N/m. This method is also fully compatible with electrophysiological measurements and presents new possibilities for the study of membrane mechanics and the creation of artificial lipid tube networks of great importance in intra- and intercellular communication.

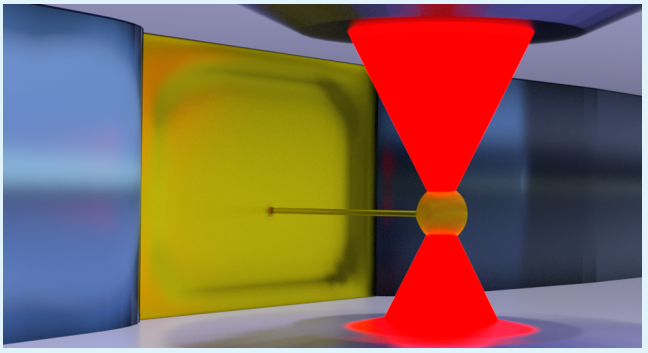

**KEYWORDS:** *cell membrane, lipid bilayer, surface tension, microdevice, lipid nanotube*

## INTRODUCTION

Mechanical forces at the cell membrane play an important role in many vital biological processes, such as endo- and exocytosis,[1−3] inter- and intracellular communication,[4] cell division,[5] and cell spreading.[6,7] A large number of these cellular processes depend on unequal conditions on each side of the membrane (e.g., proton-motive force-dependent processes). Direct measurements of these forces represent a major experimental challenge as they require the integration of force measurement techniques, such as optical tweezers, with lipid bilayers while allowing the independent control and measurement of physiological conditions, electric potential or pH, on both sides of the cell membrane.

Previous approaches have used artificial membranes, which mimic cell membranes in vitro and offer more control over physicochemical conditions than in vivo systems. Such approaches include supported lipid bilayers, black lipid membranes, and lipid vesicles.[8−10] The combination of optical tweezers with supported lipid bilayers or giant unilamellar vesicles (GUVs) has contributed to our biophysical understanding of lipid nanotube formation,[11,12] the influence of protein crowding on membrane nanotube mechanics,[13] and the role of proteins involved in membrane fission[14] and fusion.[15] However, these approaches are limited because they do not allow equal access and control over the conditions on both sides of the membrane.

Here, we present a design for an experimental platform ideally suited to the study of biological membrane processes. A free-standing membrane is formed between the two microchannels of a flow cell. Our device integrates optical tweezers

Received: June 12, 2019
Accepted: August 26, 2019
Published: August 26, 2019

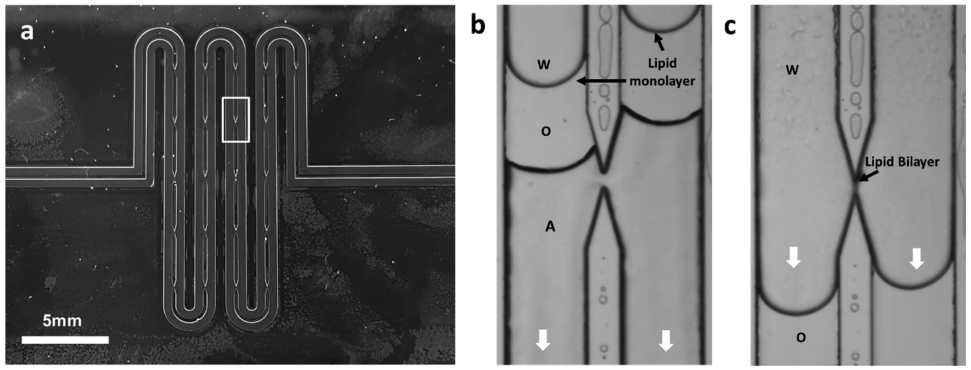


**Figure 1.** Design of the microdevice combining free-standing membranes with optical tweezers. (a) Picture of a representative microfluidic device used for mechanical measurements. Free-standing lipid bilayers are formed over the apertures connecting the two microchannels. The white square indicates the position of one of the apertures. (b, c) Pictures of the process of membrane formation (b) before the organic solvent reaches the aperture and (c) after membrane formation (A, air; O, organic phase; and W, aqueous phase; white arrows indicate the direction of the flow).

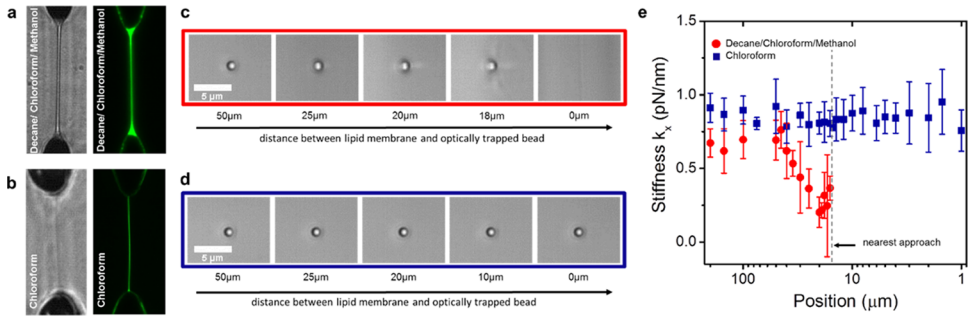


**Figure 2.** Effect of the lipid membrane annulus on optical imaging and optical trap stiffness. (a, b) Bright-field (left) and confocal fluorescence optical microscopy (right) images of lipid membranes formed using (a) a mixture of decane/chloroform/methanol as an organic solvent and (b) only chloroform as an organic solvent. (c, d) Pictures of a trapped bead near a membrane prepared using (c) decane/chloroform/methanol mixture and (d) chloroform. The distances between the bead and the membrane are indicated at the bottom of the pictures. (e) Optical trap stiffness in the *x*-axis, perpendicular to the membrane plane, as a function of the trap position with respect to the membrane. Trap stiffness measurements are all done with 1 $\mu$m beads and a laser power of 1.3 W (measured before entering the microscope objective) near the membranes formed using decane/chloroform/methanol (red circles) and chloroform (blue squares). The position represents the distance between the trap center and the membrane. The bars represent the standard deviation between measurements.

with a flow cell that provides access to both leaflets of the membrane independently, thereby affording independent and dynamic control over physiological conditions on each side of the membrane. The flow cell supports electrophysiology measurements, which we demonstrate by monitoring the capacitance of the membrane in real time. While several approaches to form free-standing membranes in microdevices are reported,[16−19] they have all been hindered by the presence of an annulus[20] of solvent generally trapped within the lipid membrane, which is responsible for severe optical aberrations[21] that prevent optical trapping close to the membrane. In contrast, we here show that the optical tweezers in our device can trap beads and accurately measure forces arbitrarily close to and on both sides of the membrane. We achieve this by reducing the presence of organic solvent between the two leaflets. The robustness of our approach and its ability to measure forces on both sides of the free-standing membrane are demonstrated by pushing optically trapped microspheres through the free-standing lipid bilayers to quantify the membrane tension and form lipid membrane nanotubes, a biologically relevant structure. This microfluidic platform is ideal for biophysical studies of biomolecules interacting with membranes. To demonstrate this, the cell-penetrating HIV-1 trans-activator of transcription (TAT) peptide[22] is introduced into the microchannel to be inserted into the membrane. We find the presence of TAT reduces the membrane tension.

## RESULTS AND DISCUSSION

**Interfacing Free-Standing Lipid Bilayers with Optical Tweezers.** The free-standing lipid membranes are formed inside a microfluidic device consisting of two parallel microchannels connected by one or several rectangular apertures of 100 $\mu$m × 85 $\mu$m (Figures 1 and S1). The lipid membranes are formed by the contact of two lipid monolayers at the water−solvent interface over the apertures connecting the two channels (Figure 1b,c). Membranes formed in these devices, as opposed to GUVs, have both sides of the membrane readily accessible. The polymer chosen for the fabrication of the device is the photopolymerized thiol-ene resin Norland Optical Adhesive 81 (NOA81) that allows the formation of rigid and transparent microdevices, compatible with optical techniques.[23−25] NOA81 is impermeable to air and water vapor,[24] thus avoiding evaporation and being a favorable candidate for the formation and long-term stability of lipid membranes. NOA81 is generally described to be compatible with organic solvents, except for chlorinated solvents like chloroform, showing in some cases a swelling of ∼30%.[23,26,27] This susceptibility for chloroform makes it a


DOI: 10.1021/acsami.9b09983
ACS Appl. Mater. Interfaces 2019, 11, 33620−33627

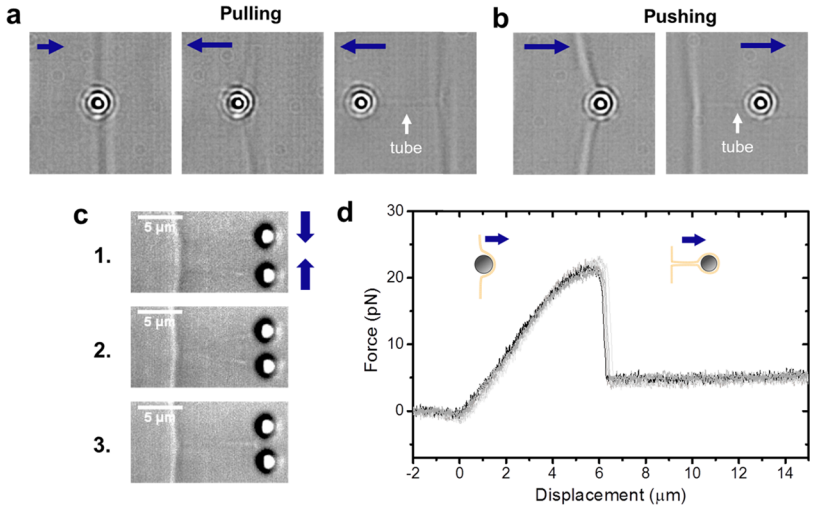


**Figure 3.** Lipid tube formation. (a) Bright-field images of a lipid tube formed by pulling a patch of membrane with an optically-trapped bead. The bead is first moved toward the membrane and then pulled away, as shown by the blue arrows. (b) Bright-field images of a lipid tube formed by pushing a bead against a free-standing lipid bilayer. (c) Bright-field images of two separate lipid tubes held by two optical traps. From top to bottom, the traps are brought closer to one another, as shown with blue arrows, until the two tubes contact and coalesce. (d) Six representative force−displacement curves obtained when pushing a 2 $\mu$m bead against the same lipid membrane.

good candidate for the preparation of membranes with a smaller annulus.

To determine whether chloroform can indeed reduce annulus size, two different approaches using different organic solvents are followed. In both approaches, 1,2-dioleoyl-*sn*-glycero-3-phosphocholine/1,2-dipalmitoyl-*sn*-glycero-3-phosphocholine (DOPC/DPPC) (2:1 molar ratio) is used as lipid component. In the first approach, lipid membranes are formed by subsequently flowing a mixture of decane/chloroform/methanol (7:2:1 v/v) and an aqueous solution containing lipids. In the second approach, membranes are prepared using the same lipid composition in chloroform followed by the aqueous solution. As shown in Figure 2a, the membranes formed with the solvent mixture decane/chloroform/methanol exhibit a thickened appearance at the edges, which corresponds to the annulus that is easily observable with bright-field and fluorescence microscopy. However, in membranes formed with chloroform (Figure 2b), no apparent annulus is observed. In fact, the accumulated chloroform residues are directly observed to shrink at the contour of the microstructures of the device, in agreement with the permeation of chloroform in NOA81 (Figure S2). The reduction of the annulus due to material permeability is in accordance with previous observations in polydimethylsiloxane (PDMS) and the known susceptibility of NOA81 to chloroform.[23,28]

Samples prepared following the two different approaches described previously, with a large or reduced annulus, are studied in combination with optical tweezers. Membranes prepared with decane/chloroform/methanol show clear optical aberrations as the trapped bead is brought toward the membranes to a point where the bead cannot be trapped anymore (Figure 2c). We find that optical trapping is hindered in the vicinity of these membranes. A decay in optical trapping stiffness is measured when the trapped bead is brought close to the membrane, as depicted by the red circles in Figure 2e. For bead−membrane distances above 50 $\mu$m, stiffness values remain relatively constant (~0.7 pN/nm), while at a distance shorter than 18 $\mu$m from the lipid bilayer, it is not possible to successfully trap a particle (Figure 2e).

On the other hand, due to the negligible size of the annulus when membranes are formed using chloroform, the trap stiffness remains almost unaffected at distances of 1−200 $\mu$m from the lipid bilayer (Figure 2e, blue squares) and the optical appearance of the beads remains unchanged (Figure 2d). This behavior is independent of the laser power used (Figure S3) and is attributed to the reduction in the optical aberrations caused by the annulus.[21] These observations confirm the importance of the solvent accumulated within the membrane and the improvement of the trapping stiffness in the vicinity of the membranes with a smaller annulus.

**Capacitance Measurements during Membrane Formation.** Our microfluidic approach enables straightforward electrophysiology measurements by simply adding electrodes in the microdevice. In this way, we investigate the membrane's electrical capacitance, which informs us about membrane formation kinetics and about whether organic solvent remains within the bilayer.[17] We find that lipid membranes with the small annulus form within a few seconds and reach a steady capacitance value 16 ± 10 s after initial contact of the lipid monolayers. The average steady capacitance value is $C_M$ = 49.2 ± 2.4 pF. The membrane is estimated to cover the full cross section of the gap (8500 $\mu m^2$) because the size of the annulus is negligible compared to the membrane surface area. Using the gap cross-sectional area for the membrane surface area results in a specific capacitance of 0.6 $\mu F/cm^2$. This value is in accordance with the specific capacitance reported for phospholipid bilayers composed of a mixture of DOPC and dioleoylphosphatidylethanolamine (DOPE).[29] A specific capacitance of 0.6 $\mu F/cm^2$ is also predicted for DPPC bilayers considering the measured dielectric constant ($\varepsilon_r$ = 3.2) and thickness (5 nm).[30] Substantial amounts of chloroform within the bilayer would result in a lower specific capacitance; therefore, there is no significant amount of solvent trapped within the leaflets.

**Lipid Nanotube Formation.** The combination of the free-standing membranes with optical tweezers enables nanomanipulation of the lipid bilayers to form nanotubes. Membrane nanotubes are a ubiquitous structure found in


DOI: 10.1021/acsami.9b09983
ACS Appl. Mater. Interfaces 2019, 11, 33620−33627

cells and used for inter- and intracellular exchange and transport.[31−34] They are also found in different cellular organelles, such as the endoplasmic reticulum,[35,36] mitochondria,[37] and Golgi apparatus.[38] In the cell, lipid nanotubes are thought to be formed by spontaneous curvature[39] but also by the application of force from molecular motors and the cytoskeleton.[40] In vitro, they are constructed in many studies via direct micromanipulation using optical tweezers interfaced with a GUV.[11,14,41,42]

Here, lipid nanotubes are formed by two different ways: (1) by pulling a membrane containing biotinylated lipids with a trapped streptavidin-coated microbead (Figure 3a) and (2) by pushing a trapped microbead across the membrane (Figure 3b). For both pulling and pushing experiments, trapped beads are displaced at 1 $\mu$m/s from or toward the membrane, respectively. The pulling approach, which is more conventional,[11,14,43] requires the addition of biotinylated lipids to the original lipid mixture of DOPC/DPPC (2:1) and the use of a streptavidin-coated microbead. In the conditions tested, this approach requires several contacts between the free-standing membrane and the bead for successful bead attachment via biotin−streptavidin bond creation. In contrast, the pushing approach results in nanotube formation in all attempts. In that case, the bead is wrapped by the membrane without the use of functionalization. With this approach, networks of lipid nanotubes with increasing complexity can be created through the use of multiple optical traps. To demonstrate this capability, we form two neighboring tubes by two optical traps and the coalescence of the tubes is observed in real time (Figure 3c). Tubes pushed from these free-standing lipid bilayers are as long as 550 $\mu$m (Video S1), limited by the width of the channels in the microdevice, suggesting that longer nanotubes may be achievable in wider channels.

**Membrane Tension Measurements.** Figure 3d shows typical force−displacement curves for a bead pushed against the free-standing bilayers. For convenience, we split the pushing process into two chronological segments: deforming the free-standing membrane and extending the nanotube. As shown in Figure 3d, the force increases monotonically with displacement during the initial phase of deformation until reaching the maximum, or overshoot, force. Then, a sharp transition occurs when the nanotube is formed, after which the force remains constant while the tube is extended. This behavior is qualitatively similar to observations reported previously for tubes pulled from a GUV,[11] where the force also increases until a sharp drop in force is observed when the tube is formed. However, for the pushing approach, the forces needed to create a tube are not defined by the patch of contact between biotinylated membrane and bead, as is the case when pulling a tube.[11] As a result, in the pulling experiments, it is not possible to directly extract the membrane tension, bending rigidity, and tube radius from the force−displacement curves alone, as energy conservation of the tube-pulling process only provides two equations for the three unknowns. Therefore, the pulling approach would require the use of additional sensors, such as micropipettes, or the assumption of one of the unknown values, such as the bending rigidity.[11] On the contrary, the pushing approach allows for a straightforward determination of the mechanical properties of the membrane since the process is independent of bond formation between the bead and membrane.

We hypothesize that for pushing the maximum force, or overshoot force, would depend on the radius of the bead, which is invariable during an experiment, unlike the patch area for pulling experiments. Figure 4a shows the force−displacement curves obtained for three different bead sizes. As shown in Figure 4b, the maximum force indeed increases proportionally with the bead diameter, while the force required for tube extension remains constant (Figure 4c) and is independent of bead size. Since the maximum force exhibits a linear relationship with bead size (Figure 4b), we expect that the relevant mechanical property resisting membrane deformation before nanotube formation is only tension. If bending rigidity contributions were significant, they would result in a nonlinear relationship between the maximum force and particle diameter.

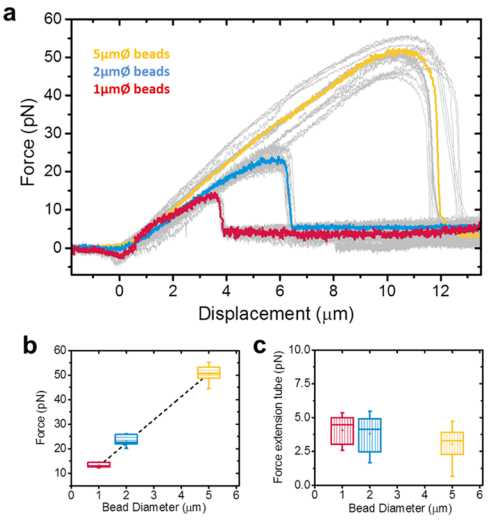


**Figure 4.** Force measurements when pushing beads of various sizes against a DOPC/DPPC lipid bilayer. (a) Force−displacement curves for tubes formed by pushing beads of 1, 2, and 5 $\mu$m diameters ($N$ = 10, 15, and 14 curves, respectively), with representative curves shown in red, blue, and yellow, respectively, and all other curves shown in gray. (b) Maximum force and (c) tube extension force as a function of bead diameter.

To model the mechanics during the pushing approach, we first consider the free-standing membrane deformation. This process is assumed to be quasi-steady since pushing speeds ranging from 0.05 to 1.0 $\mu$m/s result in overlapping force−displacement curves (Figure S4). Therefore, a force balance is conducted on the bead (Figure 5a). The two forces acting on the bead at any given time are the force $F$ from the optical tweezers and an opposing force $F_\sigma$ due to the membrane tension, which is dependent on the angle $\theta$ of the membrane at a radial distance $\delta$ from the center of the bead. An expression for this force is given by $F_\sigma = 2\pi\delta\sigma\cos\theta$, where $\sigma$ is the membrane tension. The two geometrical parameters ($\theta$ and $\delta$) are measured from videos taken during the force measurements. By balancing the forces, the surface tension can be expressed as $\sigma = \frac{F}{2\pi\delta\cos\theta}$. As shown in Figure 5b, we find that the surface tension, $\sigma$, is independent of bead size, with an average value and standard deviation of $4.63 \pm 0.74 \times 10^{-6}$ N/m. This value agrees with those obtained previously using optical methods to measure the thermal fluctuations of free-standing bilayers.[44]

From the obtained surface tension, the bending rigidity, $\kappa$, and tube radius, $R_t$, can be obtained using the force associated with nanotube extension.[45,46] The free energy of the tube


DOI: 10.1021/acsami.9b09983
ACS Appl. Mater. Interfaces 2019, 11, 33620−33627

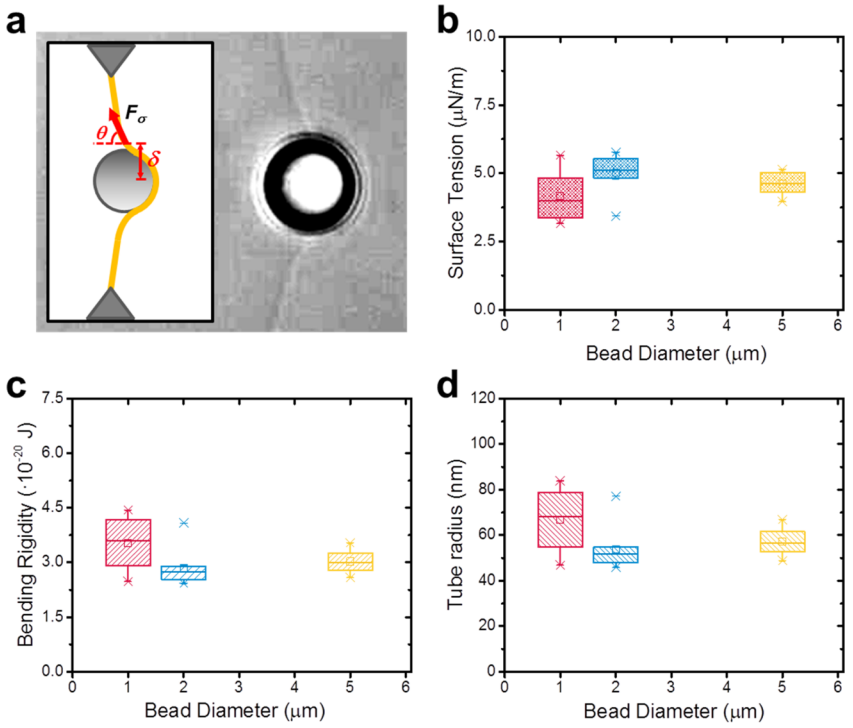


**Figure 5.** Membrane properties are extracted from force curves. (a) Representative image from video recordings used to measure the angle $\theta$ of the membrane at a radial distance $\delta$ from the center of the bead. The shown force balance is used to measure the membrane tension. (b) Membrane tension, (c) bending rigidity, and (d) radius of lipid nanotubes are not statistically different for bead diameters 1, 2, and 5 $\mu$m (Kruskal–Wallis one-way analysis of variance, $p > 0.05$).

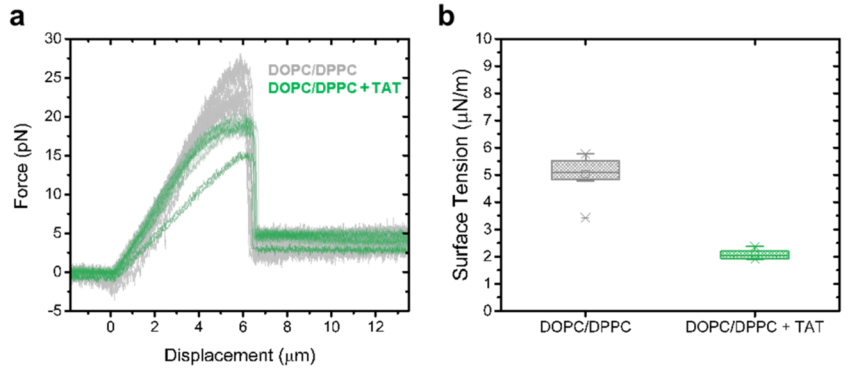


**Figure 6.** Effect of TAT peptide on membrane properties. (a) Force–displacement curves for tubes formed by pushing beads of 2 $\mu$m diameter against a DOPC/DPPC lipid bilayer without (gray) and with (green) TAT peptides, $N$ = 15 and 16 curves, respectively. (b) Membrane tension extracted from the force–displacement curves.

extension is $E_t = 2\pi R_t L_t\left(\frac{\kappa}{2R_t^2} + \sigma\right) - F_t L_t$, where $R_t$ and $L_t$ are the tube radius and length, respectively, and $F_t$ is the tube extension force.[47] As the energy must remain constant at equilibrium, the bending rigidity, $\kappa$, and surface tension, $\sigma$, are related as follows

$$\kappa = \frac{F_t^2}{8\pi^2\sigma} \quad (1)$$

With eq 1 and $R_t = \sqrt{\kappa/2\sigma}$, we find a membrane rigidity of $3.11 \pm 0.56 \times 10^{-20}$ J and a tube radius of $58.8 \pm 10.6$ nm (Figure 5c,d). The bending rigidity values obtained are within the range of those previously reported.[48]

This microfluidic platform enables studies of biomolecule–membrane interactions. To demonstrate this, an aqueous solution of the cell-penetrating HIV-1 trans-activator of transcription (TAT) peptide is injected into the microchannel to interact with the membrane. The TAT peptide is an arginine-rich peptide that has been shown to interact with lipid bilayers[49] and to carry cargo across cell membranes.[22] To characterize the interactions between the TAT peptide and membranes, we measured the tension of DOPC/DPPC membranes in the presence of TAT peptide, by pushing 2 $\mu$m beads with the optical tweezers (Figure 6). We find that the TAT peptide lowers the membrane tension to an average value and standard deviation of $2.08 \pm 0.16 \times 10^{-6}$ N/m.

## CONCLUSIONS

In summary, we introduce a microfluidic-based platform to interface free-standing membranes with optical tweezers for nanomanipulation, nanotube formation, and electrophysiolog-



DOI: 10.1021/acsami.9b09983
ACS Appl. Mater. Interfaces 2019, 11, 33620–33627

ical measurements. We use our tool to directly measure the membrane tension without assuming any values for the bending rigidity or nanotube radius. Moreover, our approach offers control over the solutions on both the outside and inside of a nanotube, where positive and negative membrane curvatures occur respectively. These are physiologically relevant membrane topologies.[50−52] For these reasons, our approach extends the range of tools available to quantify forces in cell biomechanical processes,[53] for instance, to study the mechanosensitivity associated with cell motility, auditory, and tactile functions. It also opens up new possibilities for the creation and the dynamical study of artificial lipid tube networks mimicking biological structures, i.e., lipid tubes part of cell organelles[54] and lipid tubes that extend from cells for communication.[55]

## EXPERIMENTAL SECTION

**Microfluidic Devices.** Microdevices with two parallel 100 $\mu$m-high rectangular microchannels connected with one or several apertures (Figure S1) were prepared with NOA81 (Norland Products) from PDMS molds. The PDMS molds were made by curing PDMS onto SU-8 patterns previously etched using conventional lithography. The PDMS negative replica was then gently peeled off and subsequently used as master for several NOA81 flow cells. To make the NOA81 devices, liquid NOA81 was poured onto the PDMS and covered with a clean microscope glass slide, which was treated with oxygen plasma. NOA81 was cured with UV exposition at a wavelength of 365 nm during 5 min, with 36 W of power (Promed UVL-36 with four UV-9W-L bulbs). The PDMS mold was then removed from the NOA81 microchannels, and holes were made for inlets/outlets with a drill. Then, a clean glass coverslip was spin-coated with a thin layer of NOA81, which was posteriorly partially cured by UV exposition during 30 s. The partially cured NOA81 on the coverslip and the fully cured NOA81 on the slide were gently pressed to one another to close the channels, followed by 10 min of UV exposition and heating at 80 °C during 8 h. Afterward, the channels were functionalized by flowing tri-chloro(1*H*,1*H*,2*H*,2*H*-perfluorooctyl)silane (PFOTS, Sigma-Aldrich) at 1.5% v/v in isooctane, incubated, and rinsed with isooctane and ethanol, followed by a drying and incubation step at 80 °C on a hot plate. The device with a single aperture (Figure S1a) was used for capacitance measurements, while the device with multiple apertures (Figure S1b) was used for all other assays.

**Membrane Formation.** 1,2-Dipalmitoyl-*sn*-glycero-3-phosphocholine (DPPC) and 1,2-dioleoyl-*sn*-glycero-3-phosphocholine (DOPC) in chloroform and 1,2-dipalmitoyl-*sn*-glycero-3-phosphoethanolamine-n-(cap biotinyl) (Biotinyl Cap PE) in chloroform/methanol/water, 65:35:8 v/v, were purchased from Avanti lipids. N-(Fluorescein-5-thicarbonyl)-1,2-dihexadecyl-*sn*-gycero-3-phosphoethanolamine (Fluor-DHPE) from Invitrogen Molecular Probes was used for fluorescence imaging. Free-standing membranes were formed by flowing first an organic phase, followed by an aqueous phase, with a pressure of 2 mbar (Fluigent MFCS-EZ). As mentioned in the text, two different procedures were used to prepare the planar lipid membranes. In the first approach, resulting in a thicker annulus, the organic phase consisted of ∼5 $\mu$L of a mixture of decane, chloroform, and methanol in a 7:2:1 (v/v) ratio and the aqueous solution of 10 mM 4-(2-hydroxyethyl)-1-piperazineethanesulfonic acid (HEPES) and 150 mM KCl, pH 7.4, containing 9 mg/mL DOPC/DPPC in a 2:1 molar ratio. For the second approach, for obtaining a reduced annulus, the organic phase consisted of ∼2 $\mu$L of 37.5 mg/mL DOPC/DPPC in a 2:1 molar ratio in chloroform and 10 mM HEPES and 150 mM KCl, pH 7.4, as the aqueous solution. In pulling experiments, Biotinyl Cap PE was added to the organic phase to a final concentration of 0.625 mg/mL.

**Optical Microscopy.** Fluorescence imaging of the free-standing lipid bilayer was performed by confocal microscopy using a Nikon A1R confocal with a 60× Plan Apo IR water-immersion objective, 488 nm laser, a GaAsP detector, and a detection filter 525/50. Fluor-DHPE was added to the initial lipid mixture at 0.15 mg/mL.

**Capacitance Measurements.** Total capacitance ($C_T$) was monitored during the bilayer formation with Ag/AgCl electrodes using a 200 Hz triangular signal at 100 mV peak to peak with a waveform generator (B&K Precision 4040A, 20 MHz). A DLPCA 200 (Femto) was used as amplifier and current-($I$)-to-potential convertor. After a low-pass filter with a cutoff frequency of 8 kHz, the acquisition was done by one channel of a DAQ USB-6009 (National Instruments) at a rate of 20 kHz. A second channel of the DAQ was connected to the waveform generator to precisely determine the period (2d$t$) and amplitude (d$V$) of the input signal. The capacitance computing was done using $C_T = I\mathrm{d}t/\mathrm{d}V$. The constant intrinsic capacitance of the flow cell ($C_0$) was measured before the formation of the bilayer membrane and subtracted from the total capacitance ($C_T$) to obtain the membrane capacitance ($C_M$): $C_M = C_T - C_0$. The specific membrane capacitance was calculated by dividing the membrane capacitance by its surface area. The capacitances of seven different membranes prepared with chloroform only as an organic solvent were recorded.

**Optical Tweezers Measurements.** The optical tweezers used were built similarly to previously described,[56,57] around an inverted microscope (Eclipse Ti-U, Nikon) using a 1064 nm trapping laser (YLR-10-LP-Y12, IPG Laser) and a 830 nm detection laser (LDT-830-30GC, TOPAG). Laser beams were split into two using polarizing beam splitters and focused on the sample with a 60× 1.2 NA water-immersion objective (Nikon). An acousto-optic deflector (IntraAction) was used to steer one laser trap, and a mirror mounted on a piezo holder (Newport) was used for the other trap. Bead position was monitored with back focal plane interferometry using position sensitive detectors (PSD, DL100-7-PCBA3, First Sensor). Fine positioning of the microscope stage was done with a piezostage (NANO-LPS100, Mad City Labs). Each bead was run through automated position calibration and stiffness calibration protocols.[58] Stiffness determination was calculated by the equipartition method.[59]

For the pulling experiments, 1 $\mu$m streptavidin-coated polystyrene beads (Kisker Biotech) were used. For the pushing experiments, 1, 2, and 5 $\mu$m polystyrene beads were used (purchased from Polysciences, Inc.). Beads were dispersed and used in a solution of 10 mM HEPES and 150 mM KCl, at pH 7.4, with 0.5 mg/mL bovine serum albumin (BSA). Tubes were formed by pushing the membrane at 1 $\mu$m/s (except for the results in Figure S4) and at a height of 40 $\mu$m from the bottom of the microchannels. The same conditions were used for the pulling experiments. To calculate the force applied on the bead during lipid nanotube formation, voltage signals from the PSD were preamplified and antialiased-filtered by a filter with a cutoff frequency of 500 Hz (with KROHN-HITE 3364), sampled at 1 kHz, and forces were calculated using the position and stiffness calibration data. Force vs displacement was represented with a five-point average.

To characterize the stiffness at various distances from the membrane, trap stiffness was measured using different membranes and different beads, moving the membrane at given distances from the trapped bead. For membranes prepared with the solvent mixture, 3 membranes and 41 beads were used for the measurements with a trapping laser power of 1.3 W. For membranes prepared with only chloroform as the organic phase, 7 membranes and 60 beads were used for the measurements with the same laser power (1.3 W) and 1 membrane was used for measurements at other laser powers (Figure S3).

**Video Recordings.** Videos of the experiments were captured using a CMOS camera (DCC1545M, Thorlabs GmbH) at 10 fps with a spatial resolution of 11.5 px/$\mu$m. The videos were synchronized to the force measurements with respect to the onset of motion of the piezostage. Using an open-source tracking software (Tracking by Douglas Brown, http://physlets.org/tracker/), the membrane angle $\theta$ and its radial distance $\delta$ from the center of the bead were measured on the videos. Therefore, each force measurement $F$ was attributed to a membrane angle $\theta$ and radial distance $\delta$. For each trial, 10 measurements from the video were taken when the maximum, or overshoot, force occurs.



DOI: 10.1021/acsami.9b09983
ACS Appl. Mater. Interfaces 2019, 11, 33620−33627

**Membranes with TAT Peptides.** Synthetic HIV-1 TAT protein peptide consisting of the polycationic region 49−57, Tyr-Gly-Arg-Lys-Lys-Arg-Arg-Gln-Arg-Arg-Arg, was purchased from Santa Cruz Biotechnology. Membranes were formed by first flowing 37.5 mg/mL DOPC/DPPC in a 2:1 molar ratio in chloroform, followed by 100 $\mu$M TAT peptide in 10 mM HEPES and 150 mM KCl, pH 7.4, and finally by 2 $\mu$m beads in 10 mM HEPES and 150 mM KCl, pH 7.4, with 0.5 mg/mL bovine serum albumin (BSA). The optical tweezers pushing experiments were performed as in other experiments.

## ■ ASSOCIATED CONTENT

### Supporting Information

The Supporting Information is available free of charge on the ACS Publications website at DOI: 10.1021/acsami.9b09983.

Design of the flow cells used in this study (Figure S1), pictures of the annulus (Figure S2), stiffness measurements for other laser powers (Figure S3), formation of membrane tubes at various pushing velocities (Figure S4) (PDF)

Formation and extension of a tube by pushing a bead across a free-standing membrane to the maximum possible distance inside the microchannel (Video S1) (AVI)

## ■ AUTHOR INFORMATION


### Corresponding Author

*E-mail: m.e.aubin-tam@tudelft.nl (M.A.).

### ORCID

Aurora Dols-Perez: 0000-0001-8601-5964
Victor Marin: 0000-0002-7499-623X
Guillermo J. Amador: 0000-0003-3594-125X
Roland Kieffer: 0000-0003-2337-1405
Daniel Tam: 0000-0001-5300-0889
Marie-Eve Aubin-Tam: 0000-0001-9995-2623


### Author Contributions

§A.D.-P., V.M., and G.J.A. contributed equally to this work.

### Author Contributions

The manuscript was written through contributions of all authors. All authors have given approval to the final version of the manuscript.

### Notes

The authors declare no competing financial interest.

## ■ ACKNOWLEDGMENTS

We thank Jérémie Capoulade for his assistance with confocal microscopy and Da Wei for a useful discussion. Authors A.D.-P. and G.J.A. received funding from the European Union's Horizon 2020 research and innovation programme under the Marie Skłodowska-Curie Grant agreement no. 707404. M.A. received funding from the Netherlands Organization for Scientific Research (VIDI NWO Grant 723-016-007).

## ■ ABBREVIATIONS

DOPC, dioleoylphosphatidylcholine
DOPE, dioleoylphosphatidylethanolamine
DPPC, dipalmitoylphosphatidylcholine
GUV, giant unilamellar vesicle
NOA81, Norland Optical Adhesive 81
PDMS, polydimethylsiloxane
TAT, trans-activator of transcription

## ■ REFERENCES


(1) Thottacherry, J. J.; Kosmalska, A. J.; Kumar, A.; Vishen, A. S.; Elosegui-Artola, A.; Pradhan, S.; Sharma, S.; Singh, P. P.; Guadamillas, M. C.; Chaudhary, N.; Vishwakarma, R.; Trepat, X.; del Pozo, M. A.; Parton, R. G.; Rao, M.; Pullarkat, P.; Roca-Cusachs, P.; Mayor, S. Mechanochemical Feedback Control of Dynamin Independent Endocytosis Modulates Membrane Tension in Adherent Cells. *Nat. Commun.* **2018**, *9*, No. 4217.

(2) Gauthier, N. C.; Fardin, M. A.; Roca-Cusachs, P.; Sheetz, M. P. Temporary Increase in Plasma Membrane Tension Coordinates the Activation of Exocytosis and Contraction During Cell Spreading. *Proc. Nat. Acad. Sci. U.S.A.* **2011**, *108*, 14467−14472.

(3) Apodaca, G. Modulation of Membrane Traffic by Mechanical Stimuli. *Am. J. Physiol. Renal Physiol.* **2002**, *282*, F179−F190.

(4) Wang, N.; Tytell, J. D.; Ingber, D. E. Mechanotransduction at a Distance: Mechanically Coupling the Extracellular Matrix with the Nucleus. *Nat. Rev. Mol. Cell Biol.* **2009**, *10*, 75−82.

(5) Raucher, D.; Sheetz, M. P. Membrane Expansion Increases Endocytosis Rate During Mitosis. *J. Cell. Biol.* **1999**, *144*, 497−506.

(6) Norman, L. L.; Brugués, J.; Sengupta, K.; Sens, P.; Aranda-Espinoza, H. Cell Blebbing and Membrane Area Homeostasis in Spreading and Retracting Cells. *Biophys. J.* **2010**, *99*, 1726−1733.

(7) Diz-Muñoz, A.; Fletcher, D. A.; Weiner, O. D. Use the Force: Membrane Tension as an Organizer of Cell Shape and Motility. *Trends Cell Biol.* **2013**, *23*, 47−53.

(8) Morigaki, K.; Tanimoto, Y. Evolution and Development of Model Membranes for Physicochemical and Functional Studies of the Membrane Lateral Heterogeneity. *Biochim. Biophys. Acta, Biomembr.* **2018**, *1860*, 2012−2017.

(9) Pomorski, T. G.; Nylander, T.; Cárdenas, M. Model Cell Membranes: Discerning Lipid and Protein Contributions in Shaping the Cell. *Adv. Colloid Interface Sci.* **2014**, *205*, 207−220.

(10) Lazzara, T. D.; Kliesch, T.-T.; Janshoff, A.; Steinem, C. Orthogonal Functionalization of Nanoporous Substrates: Control of 3D Surface Functionality. *ACS Appl. Mater. Interfaces* **2011**, *3*, 1068−1076.

(11) Koster, G.; Cacciuto, A.; Derényi, I.; Frenkel, D.; Dogterom, M. Force Barriers for Membrane Tube Formation. *Phys. Rev. Lett.* **2005**, *94*, No. 068101.

(12) Valentino, F.; Sens, P.; Lemière, J.; Allard, A.; Betz, T.; Campillo, C.; Sykes, C. Fluctuations of a Membrane Nanotube Revealed by High-Resolution Force Measurements. *Soft Matter* **2016**, *12*, 9429−9435.

(13) Sorre, B.; Callan-Jones, A.; Manzi, J.; Goud, B.; Prost, J.; Bassereau, P.; Roux, A. Nature of Curvature Coupling of Amphiphysin with Membranes Depends on its Bound Density. *Proc. Natl. Acad. Sci. U.S.A.* **2012**, *109*, 173−178.

(14) Roux, A.; Koster, G.; Lenz, M.; Sorre, B.; Manneville, J.-B.; Nassoy, P.; Bassereau, P. Membrane Curvature Controls Dynamin Polymerization. *Proc. Nat. Acad. Sci. U.S.A.* **2010**, *107*, 4141−4146.

(15) Brouwer, I.; Giniatullina, A.; Laurens, N.; Weering, J. R. T. v.; Bald, D.; Wuite, G. J. L.; Groffen, A. J. Direct Quantitative Detection of Doc2b-Induced Hemifusion in Optically Trapped Membranes. *Nat. Commun.* **2015**, *6*, No. 8387.

(16) Beltramo, P. J.; Hooghten, R. V.; Vermant, J. Millimeter-Area, Free Standing, Phospholipid Bilayers. *Soft Matter* **2016**, *12*, 4324−4331.

(17) Marin, V.; Kieffer, R.; Padmos, R.; Aubin-Tam, M.-E. Stable Free-Standing Lipid Bilayer Membranes in Norland Optical Adhesive 81 Microchannels. *Anal. Chem.* **2016**, *88*, 7466−7470.

(18) Zagnoni, M. Miniaturised Technologies for the Development of Artificial Lipid Bilayer Systems. *Lab Chip* **2012**, *12*, 1026−1039.

(19) Czekalska, M. A.; Kaminski, T. S.; Jakiela, S.; Tanuj Sapra, K.; Bayley, H.; Garstecki, P. A Droplet Microfluidic System for Sequential Generation of Lipid Bilayers and Transmembrane Electrical Recordings. *Lab Chip* **2015**, *15*, 541−548.

(20) Ries, R. S.; Choi, H.; Blunck, R.; Bezanilla, F.; Heath, J. R. Black Lipid Membranes: Visualizing the Structure, Dynamics, and Substrate




DOI: 10.1021/acsami.9b09983
*ACS Appl. Mater. Interfaces* 2019, 11, 33620−33627

Dependence of Membranes. *J. Phys. Chem. B* **2004**, *108*, 16040−16049.
(21) Berestovsky, G. N.; Gyulkhandanyan, M. Z.; Ivkov, V. G.; Razhin, V. D. Voltage-Induced Reflectivity Relaxation of Bilayer Lipid Membranes: On Changes of Bilayer Thickness. *J. Membr. Biol.* **1978**, *43*, 107−126.
(22) Bechara, C.; Sagan, S. Cell-Penetrating Peptides: 20 Years Later, Where Do We Stand? *FEBS Lett.* **2013**, *587*, 1693−1702.
(23) Sheppard, G.; Oseki, T.; Baba, A.; Patton, D.; Kaneko, F.; Mao, L.; Locklin, J. Thiolene-Based Microfluidic Flow Cells for Surface Plasmon Resonance Imaging. *Biomicrofluidics* **2011**, *5*, No. 026501.
(24) Bartolo, D.; Degré, G.; Nghe, P.; Studer, V. Microfluidic Stickers. *Lab Chip* **2008**, *8*, 274−279.
(25) Sollier, E.; Murray, C.; Maoddi, P.; Di Carlo, D. Rapid Prototyping Polymers for Microfluidic Devices and High Pressure Injections. *Lab Chip* **2011**, *11*, 3752−3765.
(26) Hung, L.-H.; Lin, R.; Lee, A. P. Rapid Microfabrication of Solvent-resistant Biocompatible Microfluidic Devices. *Lab Chip* **2008**, *8*, 983−987.
(27) Wägli, P.; Homsy, A.; de Rooij, N. F. Norland Optical Adhesive (NOA81) Microchannels with Adjustable Wetting Behavior and High Chemical Resistance Against a Range of Mid-infrared-transparent Organic Solvents. *Sens. Actuators, B* **2011**, *156*, 994−1001.
(28) Malmstadt, N.; Nash, M. A.; Purnell, R. F.; Schmidt, J. J. Automated Formation of Lipid-bilayer Membranes in a Microfluidic Device. *Nano Lett.* **2006**, *6*, 1961−1965.
(29) Chanturiya, A. N.; Basañez, G.; Schubert, U.; Henklein, P.; Yewdell, J. W.; Zimmerberg, J. PB1-F2, an Influenza A Virus-Encoded Proapoptotic Mitochondrial Protein, Creates Variably Sized Pores in Planar Lipid Membranes. *J. Virol.* **2004**, *78*, 6304−6312.
(30) Gramse, G.; Dols-Perez, A.; Edwards, M. A.; Fumagalli, L.; Gomila, G. Nanoscale Measurement of the Dielectric Constant of Supported Lipid Bilayers in Aqueous Solutions with Electrostatic Force Microscopy. *Biophys. J.* **2013**, *104*, 1257−1262.
(31) Gerdes, H.-H.; Bukoreshtliev, N. V.; Barroso, J. F. V. Tunneling Nanotubes: A New Route for the Exchange of Components Between Animal Cells. *FEBS Lett.* **2007**, *581*, 2194−2201.
(32) Önfelt, B.; Nedvetzki, S.; Benninger, R. K. P.; Purbhoo, M. A.; Sowinski, S.; Hume, A. N.; Seabra, M. C.; Neil, M. A. A.; French, P. M. W.; Davis, D. M. Structurally Distinct Membrane Nanotubes Between Human Macrophages Support Long-distance Vesicular Traffic or Surfing of Bacteria. *J. Immunol.* **2006**, *177*, 8476−8483.
(33) Davis, D. M.; Sowinski, S. Membrane Nanotubes: Dynamic Long-distance Connections Between Animal Cells. *Nat. Rev. Mol. Cell Biol.* **2008**, *9*, 431−436.
(34) Pande, S.; Shitut, S.; Freund, L.; Westermann, M.; Bertels, F.; Colesie, C.; Bischofs, I. B.; Kost, C. Metabolic Cross-Feeding via Intercellular Nanotubes Among Bacteria. *Nat. Commun.* **2015**, *6*, No. 6238.
(35) Leduc, C.; Campàs, O.; Joanny, J.-F.; Prost, J.; Bassereau, P. Mechanism of Membrane Nanotube Formation by Molecular Motors. *Biochim. Biophys. Acta, Biomembr.* **2010**, *1798*, 1418−1426.
(36) Cole, N. B.; Lippincott-Schwartz, J. Organization of Organelles and Membrane Traffic by Microtubules. *Curr. Opin. Cell Biol.* **1995**, *7*, 55−64.
(37) Li, T.; Zheng, F.; Cheung, M.; Wang, F.; Fu, C. Fission Yeast Mitochondria are Distributed by Dynamic Microtubules in a Motor-Independent Manner. *Sci. Rep.* **2015**, *5*, No. 11023.
(38) Polishchuk, E. V.; Di Pentima, A.; Luini, A.; Polishchuk, R. S. Mechanism of Constitutive Export from the Golgi: Bulk Flow via the Formation, Protrusion, and En Bloc Cleavage of Large Trans-Golgi Network Tubular Domains. *Mol. Biol. Cell* **2003**, *14*, 4470−4485.
(39) Liu, Y. G.; Agudo-Canalejo, J.; Grafmuller, A.; Dimova, R.; Lipowsky, R. Patterns of Flexible Nanotubes Formed by Liquid-Ordered and Liquid-Disordered Membranes. *ACS Nano* **2016**, *10*, 463−474.
(40) Raviv, U.; Needleman, D. J.; Li, Y.; Miller, H. P.; Wilson, L.; Safinya, C. R. Cationic Liposome−Microtubule Complexes: Pathways to the Formation of Two-State Lipid−Protein Nanotubes with Open or Closed Ends. *Proc. Nat. Acad. Sci. U.S.A.* **2005**, *102*, 11167−11172.
(41) Meinel, A.; Trankle, B.; Romer, W.; Rohrbach, A. Induced Phagocytic Particle Uptake into a Giant Unilamellar Vesicle. *Soft Matter* **2014**, *10*, 3667−3678.
(42) Raktim, D.; Rumiana, D. Inward and Outward Membrane Tubes Pulled from Giant Vesicles. *J. Phys. D: Appl. Phys.* **2014**, *47*, No. 282001.
(43) Karimi, M.; Steinkühler, J.; Roy, D.; Dasgupta, R.; Lipowsky, R.; Dimova, R. Asymmetric Ionic Conditions Generate Large Membrane Curvatures. *Nano Lett.* **2018**, *18*, 7816−7821.
(44) Takei, T.; Yaguchi, T.; Fujii, T.; Nomoto, T.; Toyota, T.; Fujinami, M. Measurement of Membrane Tension of Free Standing Lipid Bilayers via Laser-Induced Surface Deformation Spectroscopy. *Soft Matter* **2015**, *11*, 8641−8647.
(45) Derényi, I.; Jülicher, F.; Prost, J. Formation and Interaction of Membrane Tubes. *Phys. Rev. Lett.* **2002**, *88*, No. 238101.
(46) Evans, E.; Yeung, A. Hidden Dynamics in Rapid Changes of Bilayer Shape. *Chem. Phys. Lip.* **1994**, *73*, 39−56.
(47) Shitamichi, Y.; Ichikawa, M.; Kimura, Y. Mechanical Properties of a Giant Liposome Studied Using Optical Tweezers. *Chem. Phys. Lett.* **2009**, *479*, 274−278.
(48) Dimova, R. Recent Developments in the Field of Bending Rigidity Measurements on Membranes. *Adv. Colloid Interface Sci.* **2014**, *208*, 225−234.
(49) Chen, X.; Liu, S.; Deme, B.; Cristiglio, V.; Marquardt, D.; Weller, R.; Rao, P.; Wang, Y.; Bradshaw, J. Efficient Internalization of TAT Peptide in Zwitterionic DOPC Phospholipid Membrane Revealed by Neutron Diffraction. *Biochim. Biophys. Acta, Biomembr.* **2017**, *1859*, 910−916.
(50) De Franceschi, N.; Alqabandi, M.; Miguet, N.; Caillat, C.; Mangenot, S.; Weissenhorn, W.; Bassereau, P. The ESCRT Protein CHMP2B Acts as a Diffusion Barrier on Reconstituted Membrane Necks. *J. Cell Sci.* **2019**, *132*, No. jcs217968.
(51) Lee, I.-H.; Kai, H.; Carlson, L.-A.; Groves, J. T.; Hurley, J. H. Negative Membrane Curvature Catalyzes Nucleation of Endosomal Sorting Complex Required for Transport (ESCRT)-III Assembly. *Proc. Nat. Acad. Sci. U.S.A.* **2015**, *112*, 15892−15897.
(52) Hatzakis, N. S.; Bhatia, V. K.; Larsen, J.; Madsen, K. L.; Bolinger, P.-Y.; Kunding, A. H.; Castillo, J.; Gether, U.; Hedegård, P.; Stamou, D. How Curved Membranes Recruit Amphipathic Helices and Protein Anchoring Motifs. *Nat. Chem. Biol.* **2009**, *5*, No. 835.
(53) Roca-Cusachs, P.; Conte, V.; Trepat, X. Quantifying Forces in Cell Biology. *Nat. Cell Biol.* **2017**, *19*, 742−751.
(54) Sackmann, E. Endoplasmatic Reticulum Shaping by Generic Mechanisms and Protein-Induced Spontaneous Curvature. *Adv. Colloid Interface Sci.* **2014**, *208*, 153−160.
(55) Baker, M. How the Internet of Cells has Biologists Buzzing. *Nature* **2017**, *549*, 322−324.
(56) Brau, R. R.; Tarsa, P. B.; Ferrer, J. M.; Lee, P.; Lang, M. J. Interlaced Optical Force-Fluorescence Measurements for Single Molecule Biophysics. *Biophys. J.* **2006**, *91*, 1069−1077.
(57) Aubin-Tam, M.-E.; Olivares, A. O.; Sauer, R. T.; Baker, T. A.; Lang, M. J. Single-Molecule Protein Unfolding and Translocation by an ATP-Fueled Proteolytic Machine. *Cell* **2011**, *145*, 257−267.
(58) Lang, M. J.; Asbury, C. L.; Shaevitz, J. W.; Block, S. M. An Automated Two-Dimensional Optical Force Clamp for Single Molecule Studies. *Biophys. J.* **2002**, *83*, 491−501.
(59) Visscher, K.; Gross, S. P.; Block, S. M. Construction of Multiple-Beam Optical Traps with Nanometer-Resolution Position Sensing. *IEEE J. Sel. Top. Quantum Electron.* **1996**, *2*, 1066−1076.


DOI: 10.1021/acsami.9b09983
*ACS Appl. Mater. Interfaces* 2019, 11, 33620−33627